Optical Properties of Nanocrystalline/Amorphous TiO_2 Thin Film Deposited by rf Plasma Magnetron Sputtering

A.A. Abd El-Moula[a,b], M. Raaif[b,c,*], F.M. El-Hossary[b]

[a]Physics Department, College of Science, Jouf University, P.O. Box 2014, Sakaka, Saudi Arabia
[b]Physics Department, Faculty of Science, Sohag University, 82524 Sohag, Egypt
[c]Physics Department, Faculty of Science and Arts, Al-Mandaq, Al-Baha University, Saudi Arabia

(Received October 13, 2019; in final form March 30, 2020)

This work is a part of serious experimental efforts established on constructing multilayers based on TiO_2 for industrial use in optical devices. Recognizing the structure and optical features of TiO_2 single layer is very significant in designing optical devices and in constructing multilayers based on TiO_2 layer for probable industrial requests. In this regard, rf plasma magnetron sputtering was employed to prepare TiO_2 thin film on glass substrates. The effect of oxygen ratios % with respect to argon on the optical characteristics of TiO_2 thin film was studied. Structural studies revealed the transition from crystallization to amorphous nature of TiO_2 films with increasing the oxygen ratios. All TiO_2 thin films were transparent in the visible zone and the transmittance of TiO_2 films increased with increasing the O_2 ratios. The estimated energy gap of TiO_2 thin films increased from 3.62 eV to 3.77 eV with increasing the oxygen ratios. However, the refractive index decreased with increasing the oxygen ratios. Moreover, diverged optical constants like optical conductivity (σ_{opt}), dielectric constants (ε_i and ε_r), the Urbach energy (E_{u}), the dispersion energy (E_{d}) and single oscillator energy (E_{o}) have been explored and discussed.

DOI: 10.12693/APhysPolA.137.1068

PACS/topics: TiO_2 thin films, rf magnetron sputtering, optical properties, optical band gap

1. Introduction

Titanium dioxide (TiO_2) is a transparent semiconductor material, which is characterized by high refractive index, good transparency and wide band gap E_g of 3.0–3.2 eV. These features are influenced by amorphous, micro/nanostructure and crystallinity of TiO_2. Titanium dioxide is employed in many optical and industrial applications included but not limited; designing optoelectronic devices and solar cells [1], multilayer optical coating [2], gas sensors [3] and photocatalytic purifier [4]. Owed to its high dielectric constant, it is engaged in microelectronic devices [5]. Oxygen defects, impurities and crystallite size affected the optical features of TiO_2 thin films. Further, the preparation methods and post deposition thermal treatments play a gigantic role in inducing the desired optoelectrical properties of TiO_2 thin films. Thin films of titanium dioxide are prepared by distinct methods like sol–gel [6], chemical vapor deposition [7], electron beam evaporation [8] and sputtering methods. Uniform films with good adherence to the substrate can be produced by rf magnetron sputtering, which provides flexibility in selecting the deposition conditions. This method offers advantages of depositing films on a large-scale area, which makes it suitable for wide scope of industrial demands [9]. Significant parameters such as film thickness, film structure, oxygen partial pressure, substrate structure and temperature affected the structural, optoelectric characteristics of TiO_2 thin films.

There are many reports examining the effects of method and deposition conditions on the morphology and optical constants of TiO_2 thin films. The effect of oxygen partial pressure on the optical properties of amorphous titanium dioxide thin films deposited by dc reactive magnetron sputtering has been explored [10]. It was demonstrated that the oxygen content of the TiO_x films increased with increase in the oxygen partial pressure and the optical band gap decreased from 3.45 eV to 3.42 eV. Moreover, the influence of oxygen concentration in Ar/O_2 gas mixture on the crystalline properties of TiO_2 thin films deposited by reactive magnetron sputtering technique was investigated [11]. It was reported that the better condition to achieve of anatase phase is at $30\% O_2$ in Ar/O_2 gas mixture. It was verified for TiO_2 thin films deposited by DC reactive magnetron sputtering, the optical band gap increased from 3.21 to 3.28 eV, with film thickness of 135 nm with increase in oxygen partial pressure from 4.8×10^{-4} to 5.0×10^{-3} mbar [12]. Balakrishnan et al. [13] have deposited TiO_2 films at different oxygen partial pressures (1×10^{-5} to 3.5×10^{-1} mbar) using pulsed laser deposition. It was concluded that, with increase in the oxygen partial pressures, the band gap of the films increased from 3.20 eV to 3.60 eV and the refractive index was found to be decreased from 2.73 to 2.06 (at 550 nm).

*corresponding author; e-mail: mraaif@daad-alumni.de

In this work, rf magnetron sputtering was engaged to deposit TiO_2 thin films at different oxygen to argon ratios. Moreover, crystallographic structure formation and variations of optical parameters like refractive index n, extinction coefficient k, optical band gap E_g, optical conductivity σ_{opt}, dielectric constants ε_i and ε_r, the Urbach energy E_u, the dispersion energy E_d and single oscillator energy E_o were estimated and discussed.

2. Experimental work

2.1. Thin film preparation

TiO_2 thin films were deposited on glass substrates using a home-made rf (13.56 MHz) magnetron sputtering system. A pure titanium target (99.99%) of 30 mm diameter and 3 mm thick was engaged as a sputter target. The used gases were: pure argon (99.99%) as a sputtering gas and pure oxygen (99.99%) as a reactive gas. Firstly, the titanium target was sputtered by Ar to remove the surface oxide and surface contaminations. The commercial glass substrates were cleaned ultrasonically with acetone and deionized water then dried before inserting in the deposition chamber. All the glass slides were fixed on the substrate holder (diameter 30 mm) and the distance between the target and the substrate holder was kept fixed to be 40 mm. The target was continuously cooled by water. The sputtering system was evacuated using a diffusion pump backed by a mechanical pump to reach a base pressure of 5×10^{-5} mbar. The sputtering process was performed in Ar/O_2 gas mixture at a fixed total pressure of about 5×10^{-3} mbar. All working parameters were fixed except the ratios of O_2 to Ar, which was varied from 10 to 50%. The deposition rate of all samples was adjusted to be 0.02 nm/s and the film thickness was fixed for all samples to be around 80 nm and the operating power was 300 W.

2.2. Thin film characterization

X-ray diffraction (XRD) was conducted to investigate the structure of the deposited films. Philips X-ray diffractometer with Cu K_α radiation in θ–2θ range from 10° to 80° with grazing incidence of 2° and step interval of 0.1° was employed in this regard. The surface morphologies of TiO_2 thin film were investigated by scanning electron microscope (FEI Company, USA). The optical transmittance and reflectance of the films were measured by means of UV–VIS–NIR spectrophotometer (JASCO V-670) in the wavelength range between 200 and 2500 nm. The thicknesses of the film were measured using a Form Talysurf 50 profilometer.

3. Results and discussion

3.1. Microstructure

Figure 1 represents the X-ray diffraction patterns of TiO_2 thin films at different ratios of oxygen (10, 20, 40, and 50%). It was observed that at low oxygen ratio

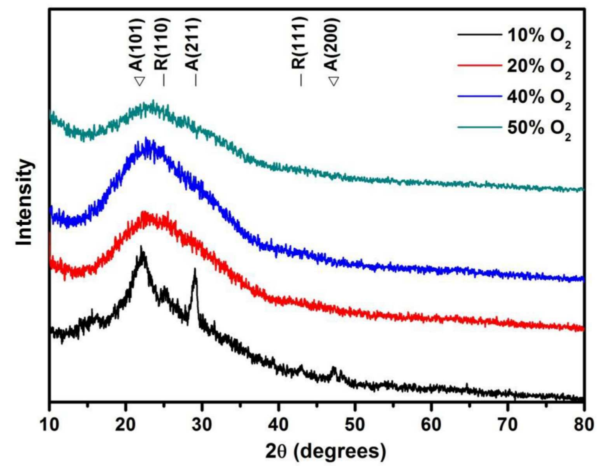

Fig. 1. The X-ray diffraction patterns of TiO_2 thin films deposited at different oxygen ratios, A and R represent anatase and rutile TiO_2 structure, respectively.

of 10% O_2, the XRD revealed a semicrystalline structure which contains a mixture of anatase (A) and rutile TiO_2 structure (R). All peaks were indexed according to JCPDS data cards no. 0021-021-1272, 00-021-1276 and 01-084-1284. The rutile phase is typically characterized, as high temperature TiO_2 phase and therefore compared to anatase it needs higher deposition energies [14]. It was demonstrated that for magnetron sputtering processes when the substrate was not heated, the energy and flux of the particles incident at the substrate could control the film structure and the existence of crystalline phases [13]. There are many factors affecting the energy provided to the growing film as total pressure, partial pressure of oxygen, deposition rate and film thickness. It was reported for TiO_2 thin film that at low partial pressure of oxygen, the crystalline structure was a predominated structure. Nevertheless, the presented results show the absence of any sharp diffraction peaks in the samples that have oxygen ratios of 20, 40 and 50%, where the deposited films revealed the amorphous structure. By increasing oxygen ratios with respect to argon to 50% O_2, the sputtered species suffered from more collisions with oxygen in which the kinetic energy of the sputtered species was reduced. Consequently, the mobility of the ad-atoms was decreased and the probability of the formation of amorphous films was increased. This observation was reported in preparing TiO_2 thin film by pulsed laser deposition [15]. Moreover, the amorphous structure of TiO_2 thin films is ascribed to low surface mobility of the deposition particles [16]. Hence, there is a transition from crystalline to amorphous structure with increase in the oxygen ratios with respect to argon during the deposition.

Crystallite size was estimated using the Debye–Scherrer formula [17] as follows:

$$D_{avg} = \frac{0.94\lambda}{\beta \cos\theta b}, \quad (1)$$

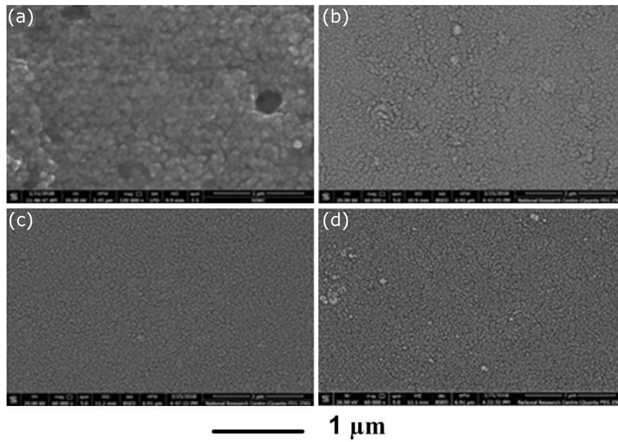

Fig. 2. The surface morphology of thin films of TiO_2 deposited at different oxygen ratios (a) 10%, (b) 20%, (c) 40%, and (d) 50%O_2.

where β is full width at half maximum in radians, D_{avg} is the average crystallite size, θ_b is the Bragg angle in degrees, and λ is the X-ray wavelength ($\lambda = 0.15406$ nm) for Cu K_α. The crystallite size for the sample deposited at oxygen ratio of 10% O_2 recorded a value of 20 nm.

Figure 2a–d shows the SEM surface morphology of TiO_2 prepared at oxygen ratios of 10, 20, 40 and 50%, respectively. The SEM image of the sample deposited at low oxygen ratio (10% O_2) revealed the presence of well-defined and spherical nanoparticles with average grain size of 30–35 nm resulting from high energy condensing particles, which have relatively high surface mobility [18]. However, The TiO_2 deposited at oxygen ratios of 20, 40, and 50%, confirmed the amorphous structure, which is in coincidence with the XRD results.

3.2. Optical properties

Figure 3a and b shows the transmittance and reflectance values of TiO_2 thin films as a function of incident light wavelength and at different oxygen ratio %. It was observed from Fig. 3a that all TiO_2 thin films were transparent in the visible region and the transmittance increased with increase in the O_2 ratios %. Many factors can affect the film transmittance such as polycrystallinity, film thickness, porosity and surface roughness. The reduction in TiO_2 film transmittance at low oxygen ratio indicated that the films have more oxygen vacancies and consequently absorption centers. The increased oxygen ratio with respect to argon confirms that the adequate oxygen can reduce the oxygen vacancies and optical scattering in the films leading to high transmittance, which is in agreement with other oxide films deposited using rf magnetron sputtering [19]. It can be seen in Fig. 3b that the reflectance increased in the region of decreasing the transmission. Moreover, the top of transmittance were coinciding with the bottom of reflectance.

3.3. Optical band gap

The absorption coefficient α was determined from the following equation [20]:

$$\alpha = d^{-1} \ln\left(\frac{1}{T}\right), \tag{2}$$

where d is the thickness of the film, T is the transmittance. The relation between absorption coefficient and photon energy $(\lambda\nu)$ is

$$(\alpha h\nu) = A(h\nu - E_g)^n, \tag{3}$$

where A is constant, h is the Planck constant, ν is the frequency of radiation, E_g is the optical band gap and n depends on the kind of transitions. For direct transition $n = 1/2$ and for indirect transition n is equal to 2. In TiO_2 thin films, according to previously reported results the absorption has an indirect transition ($n = 2$) [21]. The optical band gaps E_g were calculated by extrapolating the linear part of the intercept onto the energy axis.

It was found that the estimated energy gap of TiO_2 thin films as plotted in Fig. 4 increased with increase in oxygen ratios with respect to argon from 3.62 eV to 3.77 eV. This behavior is attributed to the variance in film composition and phase formations. Moreover, as oxygen ratios increased, oxygen defects decreased and that causes an increase in energy band gap [22]. The obtained optical band gap for the film deposited at 10% O_2

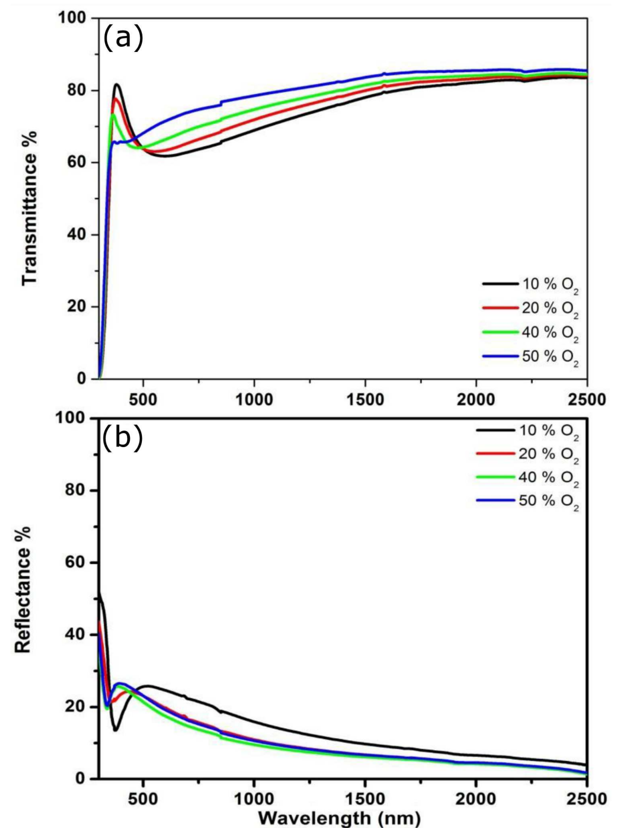

Fig. 3. Transmittance (a) and reflectance (b) spectra of TiO_2 thin films deposited at different oxygen ratios.

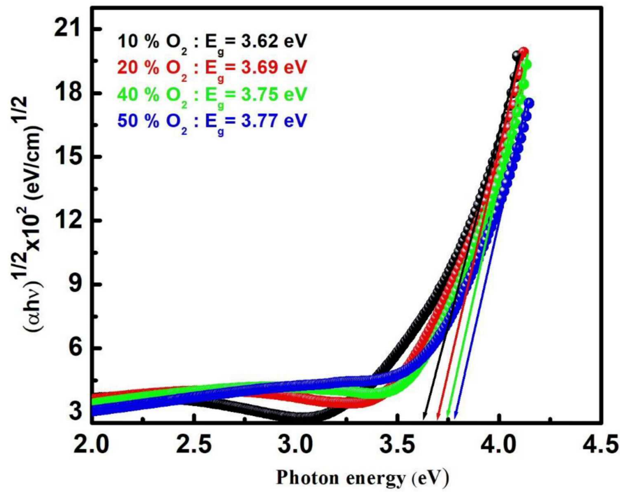

Fig. 4. The optical band gap of TiO_2 thin films deposited at different oxygen ratios.

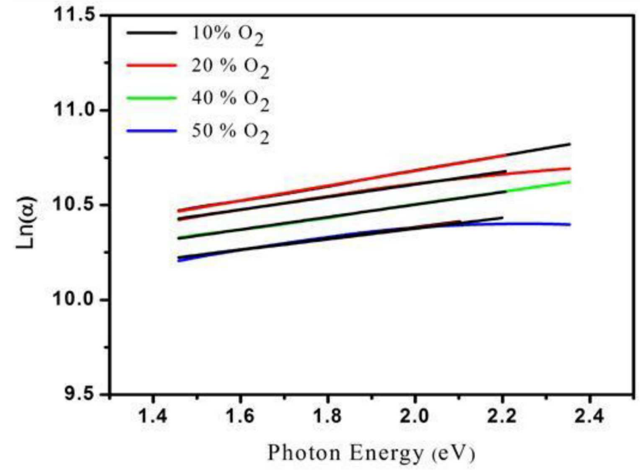

Fig. 5. The dependence of $\ln(\alpha)$ of TiO_2 thin films deposited at different oxygen ratios upon the photon energy $h\nu$.

is greater than the bulk band gap, which indicates the formation of nanoparticles [8]. The optical properties of TiO_2 films were studied by Ben Amor et al. [23] and found the direct optical transition in the range 3.3–3.5 eV. In addition, Li-Jian Meng and dos Santos [24] found that E_g of TiO_2 films increased from 3.30 eV to 3.37 eV as the oxygen partial pressure changed from 3.4×10^{-4} mbar to 3×10^{-3} mbar. Horprathum et al. [12] studied the optical properties of TiO_2 films as a function of oxygen pressure and reported that the optical band gap of TiO_2 thin films increased with increase in oxygen partial pressure from 3.21 eV to 3.28 eV.

3.4. The Urbach energy

The Urbach tail is the exponential part of the absorption coefficient curve. The Urbach tail owing to localized states appears in disordered, poor crystalline and amorphous materials. The Urbach tail energy is estimated as [25]:

$$\alpha = \alpha_0 \exp\left(\frac{hv}{E_u}\right), \tag{4}$$

$$\ln(\alpha) = \ln(\alpha_0) + \frac{hv}{E_u}, \tag{5}$$

where α_0 is a constant, and E_u is the Urbach energy (the band tail width), and it weakly depends on temperature and strongly on structural disorder.

E_u of the TiO_2 thin films was determined from the slopes of straight lines of the plot $\ln(\alpha)$ versus $h\nu$ as shown in Fig. 5. The values of E_u were listed in Table I. It was observed that the Urbach energy decreased with increase in O_2 ratios with respect to argon and this behavior is in contrast to optical band gap. It is known that the optical band gap is inversely related to the film disorder. Therefore, the reduction in estimated E_u values is attributed to the increase in E_g values. Besides, the reduction in Urbach energy results from the decrease of oxygen vacancies [26]. Moreover, the E_u values recorded in Table I are in the range of the amorphous materials [27]. These values of E_u tail confirmed the XRD results, which reflected amorphous and weak crystalline phases.

TABLE I

The calculated Urbach energy, E_d, E_o and E_g^{WD} of TiO_2 thin film deposited at different oxygen ratios %.

Oxygen ratio [%]	Urbach energy E_u [meV]	E_d [eV]	E_o [eV]	E_g^{WD} [eV]
10	341	10.91	4.58	3.05
20	304	13.17	4.74	3.16
40	299	23.66	4.97	3.31
50	254	24.39	5.12	3.41

3.5. The refractive index and extinction coefficient (n, k)

The important key for the optical devices designing is the refractive index parameter. The refractive index n is noticeably significant in designing the integrated optical devices, such as filters, switches and modulation.

The refractive index of a film is calculated according to

$$n = \frac{1+R}{1-R} + \sqrt{(R+1/R-1)^2 - (1+k^2)}. \tag{6}$$

Figure 6 presents the refractive index of TiO_2 as a function of oxygen ratios with respect to argon. It was revealed that the refractive index decreased with increased oxygen ratios. This behavior is correlated to carrier concentrations whereas a decrease in oxygen vacancies leads to a decrease in carrier concentrations. In this regard, the refractive index decreased with carrier concentrations [28]. The refractive indices of the films decreased from 2.7 to 2.29 (at 550 nm) as the oxygen ratios increased from 10 to 50%. Due to the amorphous structure of the films developed in this work, the value of the

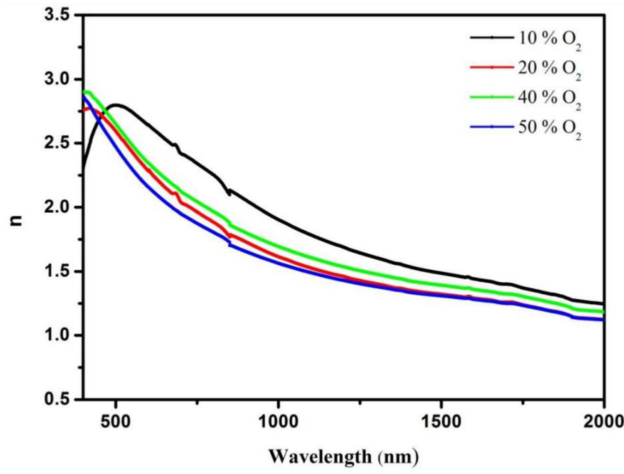

Fig. 6. The refractive index n of TiO_2 thin films deposited at different oxygen ratios.

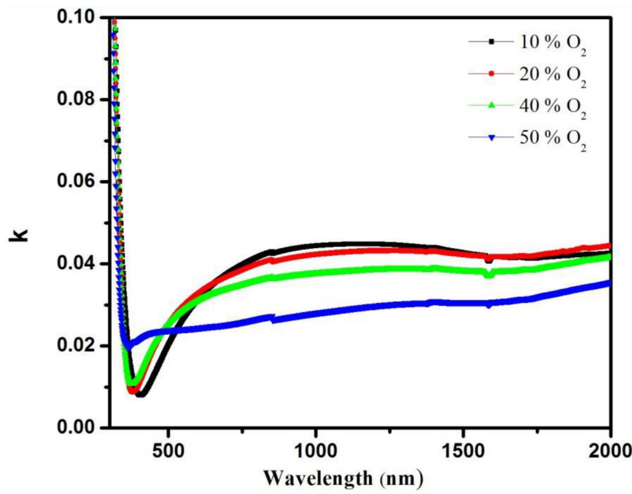

Fig. 7. The extinction coefficient k of TiO_2 thin films deposited at different oxygen ratios.

refractive index at $\lambda = 632.8$ nm is smaller than the characteristic value for the anatase phase of TiO_2, which is reported to be ≈ 2.5 [29]. Moreover, the refractive index is reduced with increase in the wavelength for all TiO_2 thin films, which display normal dispersion behavior [23].

The extinction coefficient k of a film was calculated using the relation [9]:

$$k = \frac{\alpha\lambda}{4\pi} = \frac{\lambda}{4\pi d}\ln(1/T), \tag{7}$$

where α is the absorption coefficient calculated from $\alpha = (1/d)\ln(1/T)$, where d is the thickness of film and T is transmission of the films. Figure 7 shows the extinction coefficient variations of TiO_2 thin films deposited at different ratios of oxygen. It was observed that the extinction coefficient decreased with increase in oxygen ratios, which is attributed to the decrease in surface roughness as O_2 ratios increased. Moreover, the extinction

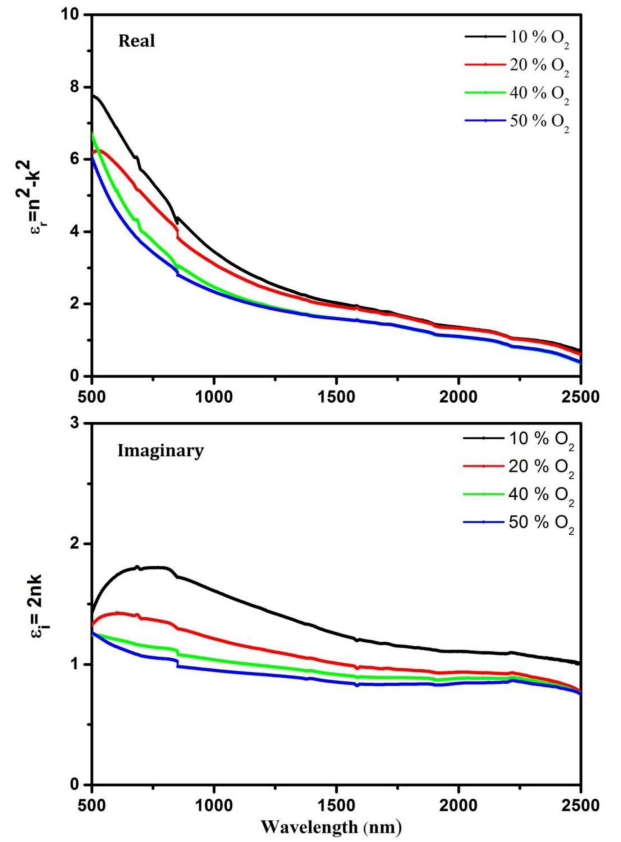

Fig. 8. Real and imaginary part of dielectric constant of TiO_2 thin films deposited at different oxygen ratios.

coefficient is correlated to the variation of optical transmittance, which increases with the decrease of scattering losses, hence decrease of the absorption coefficient. This assumption is in agreement with the transmittance data.

3.6. The dielectric constants and optical conductivity

The fundamental essential optical properties of thin films is described by the complex refractive index ($N = n + \mathrm{i}k$) and the dielectric constant which is considered as another important optical parameter and is defined as ($\varepsilon = \varepsilon_r + \mathrm{i}\varepsilon_i$). The real and imaginary portions of dielectric constant are determined by n and k values. These parameters are calculated by

$$\varepsilon_r = n^2 - k^2, \tag{8}$$

$$\varepsilon_i = 2nk, \tag{9}$$

where n and k are the refractive index and the extinction coefficient, respectively. The real part of dielectric constant give impression about the ability of the thin film to slack the speed of light, while the imaginary part describes the capability of a dielectric material to absorb energy from an electric field owed to the dipole motion.

The variations of both two parts of dielectric constants with wavelength are shown in Fig. 8. It is obvious that the variation of ε_r follows the similar trend as that observed for real part of refractive index and the variation

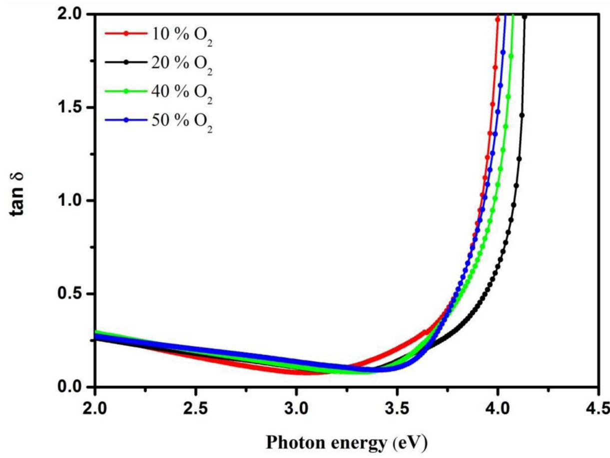

Fig. 9. Dissipation factor of TiO_2 thin films deposited at different oxygen ratios.

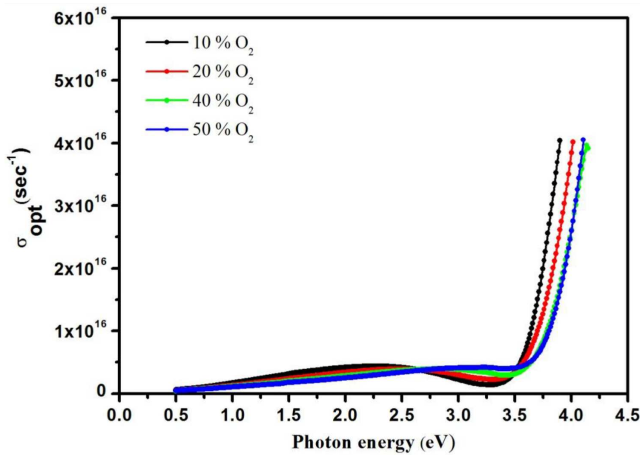

Fig. 10. Optical conductivity vs. photon energy of TiO_2 thin films deposited at different oxygen ratios.

of imaginary part ε_i is in line with the extinction coefficient k with the incident wavelength. It is clear that the values of the real part of dielectric constant are greater than the imaginary part. This is attributed to the values of ε_r are strongly depends on the refractive index where $n > k$. The values of ε_i depend mainly on k values where the small values of k reduce the values of nk product. Knowing the two parts of the dielectric constant gives information about the loss factor, which represents the ratio of the imaginary part to the real part of the dielectric constant [20]:

$$\tan\delta = \frac{\varepsilon_i}{\varepsilon_r}). \quad (10)$$

Figure 9 represents the variation of loss factor $\tan\delta$ with wavelength. It was observed the the loss factor decreased sharply with increase in the wavelength within the range from 300 to 400 nm and then it increased slightly. Moreover, the dissipation factor decreased with increasing the oxygen ratios. This may be attributed to the film density and film absorption.

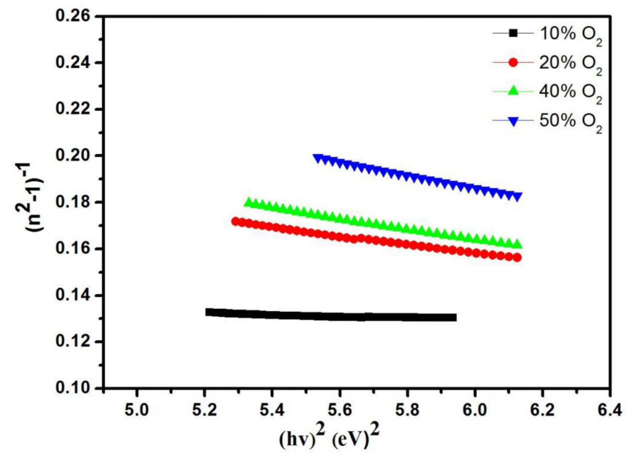

Fig. 11. Plot of the refractive index $(n^2-1)^{-1}$ vs. $(h\nu)^2$ to obtain single oscillator energy E_o and dispersion energy E_d for TiO_2 thin films deposited at different oxygen ratios.

The optical conductivity σ_{opt} is estimated using absorption coefficient α as follows [20]:

$$\sigma_{opt} = \frac{\alpha n c}{4\pi}, \quad (11)$$

where n is the refractive index and c is the velocity of light. Figure 10 represents the diversity of σ_{opt} for TiO_2 thin films deposited at different oxygen ratios of 10, 20, 40, and 50%. The figure shows that the optical conductivity σ_{opt} increased with increase in the photon energy, which is due to the electrons excited by photon energy [30]. Moreover, the optical conductivity decreased with increase in the oxygen ratios to 50%, where TiO_2 is considered as n-type semiconductor, so oxygen vacancies and titanium interstitials act as donor defects, which cause the deficit of oxygen in TiO_{2-x} [26]. Hence, at low oxygen ratios the effect of oxygen vacancies on the carrier density causes maximum conductivity, which decreases with increases of oxygen ratios [31].

3.7. Dispersion energy parameters

The dispersion energy is important for communication and spectral analysis device design. E_d and E_o are two parameters introduced by Wemple and DiDomenico [32], where E_d is the dispersion energy and represents the oscillator strength of the interband transition and determines the dispersion of the refractive index, E_o is single oscillator energy and equal to the average interband transition energy. Both the two parameters can be calculated from the relation

$$\left(n^2-1\right) = \frac{E_d E_o}{E_o^2 - (h\nu)^2}, \quad (12)$$

where n is the refractive index. By plotting $(n^2-1)^{-1}$ vs. $(h\nu)^2$ and fitting the data a straight line is obtained as shown in Fig. 11. E_o and E_d are determined directly from fitting the straight-line $(E_o E_d)^{-1}$ and the intercept E_o/E_d. The calculated values of E_o and E_d are presented in Table I. The oscillator energy E_o is related to

the optical band gap, by $E_o \approx 1.5E_g^{WD}$ as suggested by Wemple and Didomenico (WD) model. E_{gopt} is obtained in the absorption region while E_g^{WD} is determined in the transparent region. The E_d values increase with increase in the oxygen ratios, which could be attributed to the increase in the co-ordination number of the atoms resulting from the transformation of TiO_2 thin films from crystalline to amorphous structure as shown in XRD figure and as reported with other literature [33].

4. Conclusions

The effect of oxygen ratios % with respect to argon on structural and optical properties of TiO_2 thin films prepared by rf magnetron sputtering were studied. X-ray diffraction study revealed the transition from crystallization to amorphous nature of TiO_2 films with increasing ratios of oxygen. The transmittance of the TiO_2 films was found to be increased with increase in the oxygen ratios % with respect to argon owed to the decrease in oxygen vacancies. The energy band gap values are found to be increased from 3.62 to 3.77 with oxygen ratios. Various optical parameters such as n, k, ε_r and ε_i, $\tan\delta$, σ_{opt}, E_u, E_o, E_d have been explored and discussed. The results reveal that all optical parameters (E_u, α, ε_i, ε_r, and σ) decreased with increase in the oxygen ratio. These results can be used as a guide for researcher and industrialists in designing of device that are based on metal/semiconductor layers, such as solar cell and diodes. Moreover, it can be used in designing multilayers based on TiO_2 layer.

References

[1] G. Karwasz, A. Miotello, E. Zomer, R. Brusa, B. Kościelska, C. Armellini, A. Kuzmin, *Acta Phys. Pol. A* **107**, 977 (2005).

[2] N. Sarıca, Z.Z. Öztürk, C. Bindal, A.H. Üçışık, *Acta Phys. Pol. A* **129**, 759 (2016).

[3] H. Tang, K. Prasad, R. Sanjinés, F. Lévy, *Sens. Actuat. B Chem.* **26**, 71 (1995).

[4] S. Takeda, S. Suzuki, H. Odaka, H. Hosono, *Thin Solid Films* **392**, 338 (2001).

[5] W.D. Brown, W.W. Grannemann, *Solid State Electron.* **21**, 837 (1978).

[6] A. Aidla, T. Uustare, A.-A. Kiisler, J. Aarik, V. Sammelselg, *Thin Solid Films* **305**, 270 (1997).

[7] D. Bhattacharyya, N.K. Sahoo, S. Thakur, N.C. Das, *Thin Solid Films* **360**, 96 (2000).

[8] D. Pjević, T. Marinković, J. Savić, N. Bundaleski, M. Obradović, M. Milosavljević, M. Kulik, *Thin Solid Films* **591**, 224 (2015).

[9] F.M. El-Hossary, N.Z. Negm, A.M. Abd El-Rahman, M. Raaif, A.A. Abd Elmula, *Adv. Chem. Eng. Sci.* **5**, 1 (2015).

[10] Yongfeng Ju, Lin Li, Zhiming Wu, Yadong Jiang, *Energy Proced.* **12**, 450 (2011).

[11] H. Toku, R.S. Pessoa, H.S. Maciel, M. Massi, U.A. Mengui, *Surf. Coat. Technol.* **202**, 2126 (2008).

[12] M. Horprathum, P. Eiamchai, P. Chindaudom, A. Pokaipisit, P. Limsuwan, *Proced. Eng.* **32**, 676 (2012).

[13] G. Balakrishnan, Vengala Rao Bandi, S.M. Rajeswari, N. Balamurugan, R. Venkatesh Babu, J.I. Song, *Mater. Res. Bull.* **48**, 4901 (2013).

[14] J. Šícha, D. Heřman, J. Musil, Z. Strýhal, J. Pavlík, , *Plasma Process. Polym.* **4**, S345 (2007).

[15] Y. Shen, H. Yu, J. Yao, S. Shao, Z. Fan, H. He, J. Shao, *Opt. Laser Technol.* **40**, 550 (2008).

[16] L.V. Azaroff, in: *Elements of X-ray Crystallography*, McGraw-Hill, New York 1968.

[17] L. Kumari, G.H. Du, W.Z. Li, R. Selva Vennila, S.K. Saxena, D.Z. Wang, *Ceram. Int.* **35**, 2401 (2009).

[18] A. Faheem Khan, M. Mehmood, S.K. Durrani, M.L. Ali, N.A. Rahim, *Mater. Sci. Semicond. Process.* **29**, 161 (2015).

[19] C.H. Heo, S.B. Lee, J.H. Boo, *Thin Solid Film* **475**, 183 (2005).

[20] B. Astinchap, R. Moradian, K. Gholami, *Mater. Sci. Semicond. Process.* **63**, 169 (2017).

[21] S.H. Mohamed, O. Kappertz, J.M. Ngaruiya, T.P. Leervad-Pedersen, R. Drese, M. Wutting, *Thin Solid Films* **429**, 135 (2003).

[22] A.K. Kunti, M. Chowdhury, S.K. Sharma, M. Gupta, R.J. Chaudhary, *Thin Solid Films* **629**, 79 (2017).

[23] S. Ben Amor, G. Baud, J.P. Besse, M. Jacquet, *Mater. Sci. Eng. B* **47**, 110 (1997).

[24] Li-Jian Meng, M.P. dos Santos, *Appl. Surf. Sci.* **68**, 319 (1993).

[25] F. Urbach, *Phys. Rev.* **92**, 1324 (1953).

[26] J. Nowotny, C.C. Sorrell, T. Bak, L.R. Sorrell, in: *Materials for Energy Conversion Devices*, Woodhead, Cambridge, UK 2005, p. 84.

[27] A.F. Wells, *Structural Inorganic Chemistry*, 5th ed., Clarendon Press, Oxford 1984.

[28] H.M. Ali, M.M. Abou-Mesalam, M.M. El-Shorbagy, *J. Phys. Chem. Solids* **71**, 51 (2010).

[29] W.L. Bragg, A.B. Pippard, *Acta Crystallogr.* **6**, 865 (1953).

[30] Y.A.K. Reddy, I.-K. Kang, Y.B. Shin, H.Ch. Lee, P.S. Reddy, *Mater. Sci. Semicond. Process.* **32**, 107 (2015).

[31] F. Yakuphanoglu, A. Cukurovali, I. Yilmaz, *Opt. Mater.* **27**, 1363 (2005).

[32] S.H. Wemple, M. DiDomenico, *Phys. Rev. B* **3**, 1338 (1971).

[33] K.S. Usha, R. Sivakumar, C. Sanjeeviraja, *J. Mater. Sci. Mater. Electron.* **26**, 1033 (2015).